THE BELL SYSTEM
TECHNICAL JOURNAL
DEVOTED TO THE SCIENTIFIC AND ENGINEERING
ASPECTS OF ELECTRICAL COMMUNICATION

Volume 52 April 1973 Number 4

Normal Modes in Overmoded Dielectric-Lined Circular Waveguide

By J. W. CARLIN and P. D'AGOSTINO

(Manuscript received October 30, 1972)

The propagation constants (loss and phase) are determined for the normal modes in dielectric-lined overmoded (guide radius ≫ wavelength) circular guide by numerical solutions of the appropriate characteristic equations. It is shown that the heat loss of the TM_{pn} modes is quite low and decreases with increasing frequency in contrast to the increase in heat loss predicted by the perturbation theory for thin linings. The primary effect of the low-loss TM_{pn} modes on a transmission system using the TE_{01} mode is a reduction in the route bend losses.

1. INTRODUCTION

Communications systems are currently under development by the Bell System and abroad which utilize as the transmission medium dielectric-lined circular waveguide (DLG) excited in the low-loss circular electric (TE_{01}) mode. The presence of a thin dielectric liner, bonded to the wall of the waveguide, eliminates the undesirable degeneracy which exists between the phase constants of the TE_{01} and TM_{11} modes in unlined metallic guide. It also significantly modifies the propagation constant (phase and attenuation) and field distribution of many other modes compared to their counterparts in unlined waveguide.

In order to determine the TE_{01} transmission characteristics of lined waveguide, it is necessary to determine the characteristics of the normal modes of the structure. The general problem of determination of the modes in a hollow, perfectly conducting metallic cylinder with a lossless dielectric lining has been of much interest since the initial investigations of Bucholz[1] and Wachowski and Beam.[2]

Unger[3,4] discusses the basic propagation characteristics of a thinly lined DLG suitahle for use as a wide-hand carrier in the millimeter-wave region. He determines the phase velocities of the normal modes exactly, but uses a first-order perturbation theory, with lining thickness as the perturbation parameter, to ohtain the heat loss of the normal modes of DLG. It can be shown that the actual heat loss characteristics of the normal modes of DLG differ significantly from those predicted by the simple perturbation theory for a thin lining, in that modes not of the circular electric class may have very low heat loss at high frequencies. This was discussed hriefly in an earlier paper[5] which treated the loss characteristics of circular symmetric modes (TE_{on} or TM_{on}) in DLG. The present paper is a continuation of that work with a more complete discussion of the characteristics of the normal modes in overmoded DLG. Representative values for the purely real normal-mode propagation constants based on a numerical solution of the eigenvalue equation resulting from the classical boundary value problem formulation for a lossless DLG are given. The losses were determined using two different methods. The methods ("induced current" and "wall impedance") will be explained in a later section of this paper and we will see that the results are consistent. The normal-mode loss behavior in DLG was found to have a simple physical explanation in terms of the plane wave reflection coefficient of an equivalent infinite impedance plane. Whenever possible, the algebraic details are omitted or deferred to a suitable appendix. Some plots of the electric field lines of the normal modes and the energy density distribution over the guide cross section are also given.

II. BOUNDARY VALUE PROBLEM FORMULATION

An idealization of the waveguide structure under investigation is shown in Fig. 1. It is a perfectly conducting cylinder of radius b to which a lossless dielectric of relative permittivity ϵ_r and thickness t is bonded. The interior region ($r < a$) is to be filled with an inert gas and its electrical properties are those of free-space over the frequency range of interest.

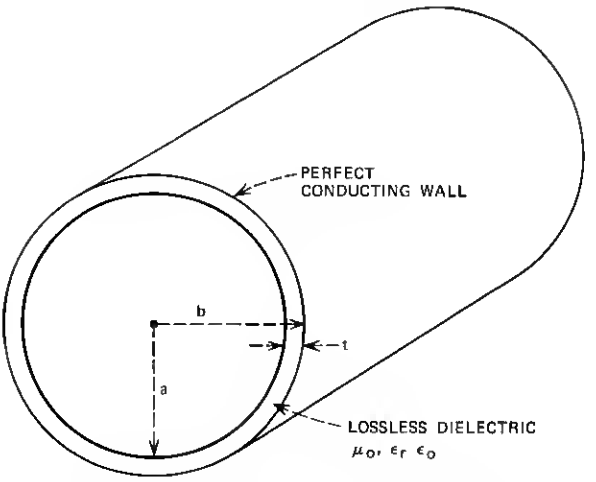

Fig. 1—The idealized lossless model for dielectric-lined guide.

The fields of a normal mode (TE_{pn} or TM_{pn}) in the structure may be expanded in the usual manner in terms of two scalar functions over the two regions of the guide cross section. In the empty region of the guide ($r < a$), they are of the form

$$\begin{aligned} T_n &= N_n J_p(\chi_n r) \sin p\phi \\ T'_n &= N_n J_p(\chi_n r) \cos p\phi \end{aligned} \qquad r < a \tag{1}$$

where N_n is a suitably chosen normalization constant. On applying the usual boundary conditions at the free-space dielectric (continuity of the tangential electric and magnetic fields) and metallic wall (zero tangential electric field) boundaries, we obtain a characteristic equation which must be solved for the eigenvalue k_n. Symbolically, we have

$$E(k_n, f, b, \epsilon_r, p, t) = 0 \tag{2}$$

where k_n (the only unknown) is defined as

$$k_n = \chi_n a, \tag{3}$$

p is the circumferential order of the mode, and f is the frequency of interest. The fields vary along the z axis as $e^{-jh_n z}$ for an assumed $e^{j\omega t}$ time dependence. The propagation constant h_n is related to k_n by

$$h_n^2 = k^2 - \chi_n^2 \tag{4}$$

where k is the free-space propagation constant.

The development of the characteristic equation is discussed by Unger[3,4] and is outlined in Appendix A for reasons of continuity. The notation used in this paper is consistent with that of Unger.[4] It should be noted that the normal mode fields corresponding to the solution of (2) are not strictly transverse electric (TE) or magnetic (TM) as in hollow metallic waveguide. (The circularly symmetric modes are pure TE or TM.) However, we carry the usual TE or TM nomenclature over with the understanding that this is what the field structure tends to in the limit of zero lining thickness.

For a lossless structure, the eigenvalue k_n as given by the solution of eq. (2) is either pure real or pure imaginary as is the characteristic eq. (2). Because of this, it is always possible to obtain a solution of (2) by the well-known "bisection" method on a digital computer.

On solving (2) for k_n, we can then determine the propagation constant h_n for the TE_{pn} or TM_{pn} mode of interest. The differential propagation constant ($\Delta\beta$) between the $TE_{pn}(TM_{pn})$ mode and the TE_{01} mode is an important parameter in the estimation of TE_{01} loss characteristics. We define $\Delta\beta$ as

$$\Delta\beta = h_n - h_{01}(\text{rad/m}). \tag{5}$$

Although the model used is an idealization of the actual lossy structure, $\Delta\beta$ as given by (5) is still an accurate representation of the difference in propagation constants. We can estimate the attenuation constant α_n(Np/m) for a $TE_{pn}(TM_{pn})$ mode by using a simple physical approximation.

The fields in the lossless structure are approximately the same as in the actual lossy guide. Hence they may be used as a very accurate first-order approximation to obtain the conduction currents in the lossy metallic walls and the displacement currents in the dielectric lining. The total heat loss (wall losses and dielectric losses) readily follows. We shall refer to this as the "induced current" method in the following discussion. The details are given in Appendix A. We now define the differential attenuation constant ($\Delta\alpha$), which is also needed to determine the TE_{01} transmission characteristics in DLG, as

$$\Delta\alpha = \alpha_n - \alpha_{01}. \tag{6}$$

In the preceding section we have indicated one well-known method of determining the attenuation and propagation constants of the normal modes in DLG. There is another approach, first introduced by Unger,[4] which aids greatly in understanding in an intuitive fashion the normal mode characteristics of DLG. This is in essence a quasi-optics ap-

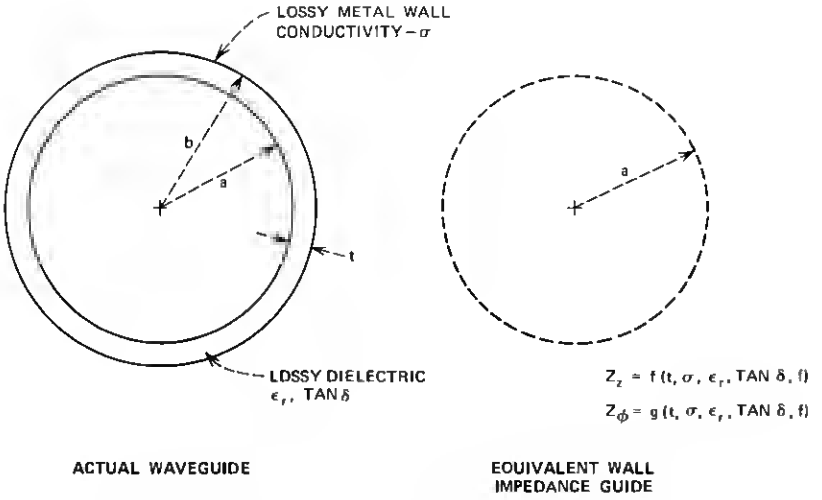

Fig. 2—The wall-impedance model for dielectric-lined guide.

proach, as we replace that portion of the DLG in the region $r > a$ of Fig. 1 by an impedance wall at $r = a$ as indicated in Fig. 2. The values of the impedances Z_z and Z_ϕ, which approximate the actual boundary conditions relating the tangential fields at the free-space dielectric boundary,

$$Z_z = -\frac{E_z}{H_\phi}\bigg| r = a,$$
$$Z_\phi = \frac{E_\phi}{H_z}\bigg| r = a, \tag{7}$$

are given by a simple plane wave analysis as outlined at the end of Section III. We can then obtain a characteristic equation for the equivalent wall-impedance structure of Fig. 2. Again we defer the details to Appendix B. The resultant equation has the form

$$E(k_n, f, Z_z, Z_\phi, a) = 0. \tag{8}$$

Here Z_z and Z_ϕ are *complex* quantities for a lossy metal wall with a lossy liner, as is the resulting eigenvalue k_n. We use the well-known Newton-Raphson method to solve (8) for k_n numerically on a digital computer. In this case, the propagation constant γ_n is complex (the fields vary along the guide axis as $e^{-j\gamma_n z}$ for $e^{j\omega t}$ time dependence) and given by

$$\gamma_n^2 = k^2 - \chi_n^2 \tag{9}$$

where

$$k_n = \chi_n a,$$

and k is the free-space propagation constant. We define the differential attenuation constant ($\Delta\alpha$) and propagation constant ($\Delta\beta$) as in (6) and (7), where it is understood that

$$\gamma_n = h_n + i\alpha_n.$$

III. RESULTS

In this section we give results characteristic of those expected of the DLG for use in typical waveguide transmission systems. The results are for a polyethylene liner bonded to copper waveguide walls. The general behavior exhibited, however, is representative of that to be expected of any low-loss dielectric liner on a good conductor.

Figure 3 is a typical plot of the eigenvalue (k_n) for the first four circular symmetric modes for the *lossless* guide of Fig. 1 based on numerical solution of the exact characteristic equation. The eigenvalues exhibit a cyclic or periodic behavior as the lining thickness increases. The eigenvalue for a $TE_{on}(TM_{on})$ mode in DLG is equal to that of a

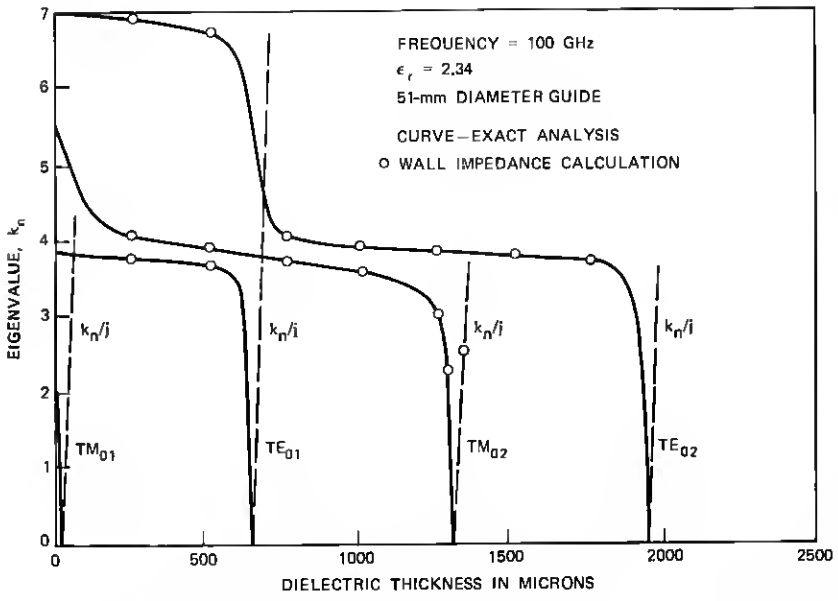

Fig. 3—Eigenvalues vs lining thickness for the TE_{on} and TM_{on} modes, lossless guide; wall-impedance model and the exact solution.

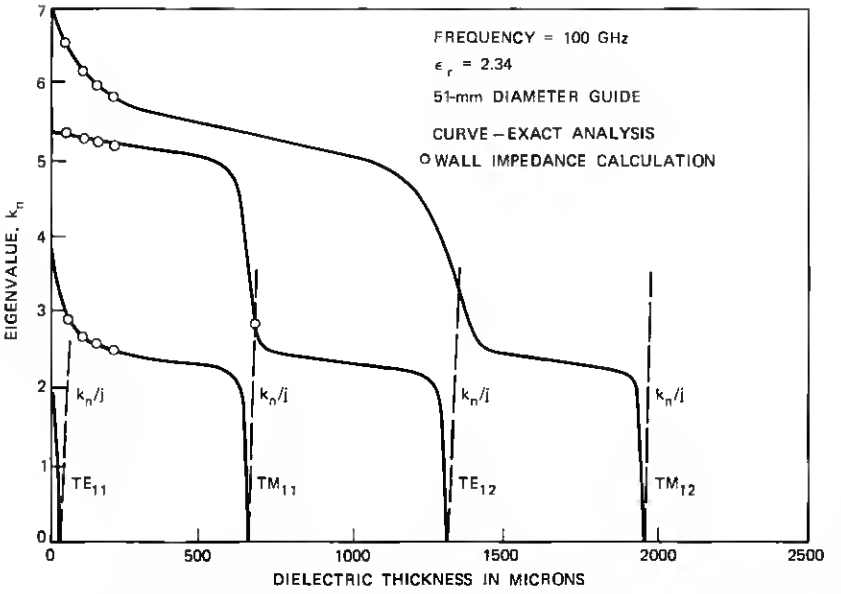

Fig. 4—Eigenvalues vs lining thickness for the TE_{1n} and TM_{1n} modes, lossless guide; wall-impedance model and the exact solution.

$TE_{o,n-1}(TM_{o,n-1})$ in unlined guide when the lining is "equivalent" to a half wavelength in thickness. The "equivalent wavelength" in the dielectric is given by $\lambda/\sqrt{\epsilon_r - 1}$, where λ is the free-space wavelength. The interested reader is referred to the discussion preceding (11) for details. Similarly, the eigenvalue for a $TE_{on}(TM_{on})$ mode in DLG is equal to that for a $TM_{o,n}(TE_{o,n-1})$ in unlined guide when the lining is a quarter-wavelength thick.

It can he seen that the eigenvalues of the TM_{on} modes change rapidly with an initial increase in lining thickness for thin linings, while those of the TE_{on} mode do not. This is due to a strong electric field at the wall for TM_{on} modes and a vanishing electric field for the TE_{on} modes.

The TM_{01} mode eigenvalue bebaves in an interesting fashion for very thin linings. It decreases rapidly to zero as the lining thickness increases and then becomes imaginary. This indicates that the TM_{01} mode propagates as a slow wave or as a surface wave closely hound to the lining region in DLG. The other circular symmetric modes exhibit the same surface wave behavior for thicker linings, i.e., a quarter-wave lining, half-wave lining, etc.

The hyhrid mode eigenvalues exhihit thc same sort of repetitive hehavior as seen in Fig. 4. Tbe eigenvalues repeat as the lining tbickness

increases by a half wavelength. The TM_{1n} eigenvalues change rapidly as the lining thickness increases for thin linings and then undergo little further change until the lining is a quarter-wave thick. The TE_{11} eigenvalue drops to zero and then becomes imaginary for very thin linings, indicative of a surface-wave-type mode. The TE_{1n} mode eigenvalues ($n > 1$) change very little for thin linings but undergo rapid

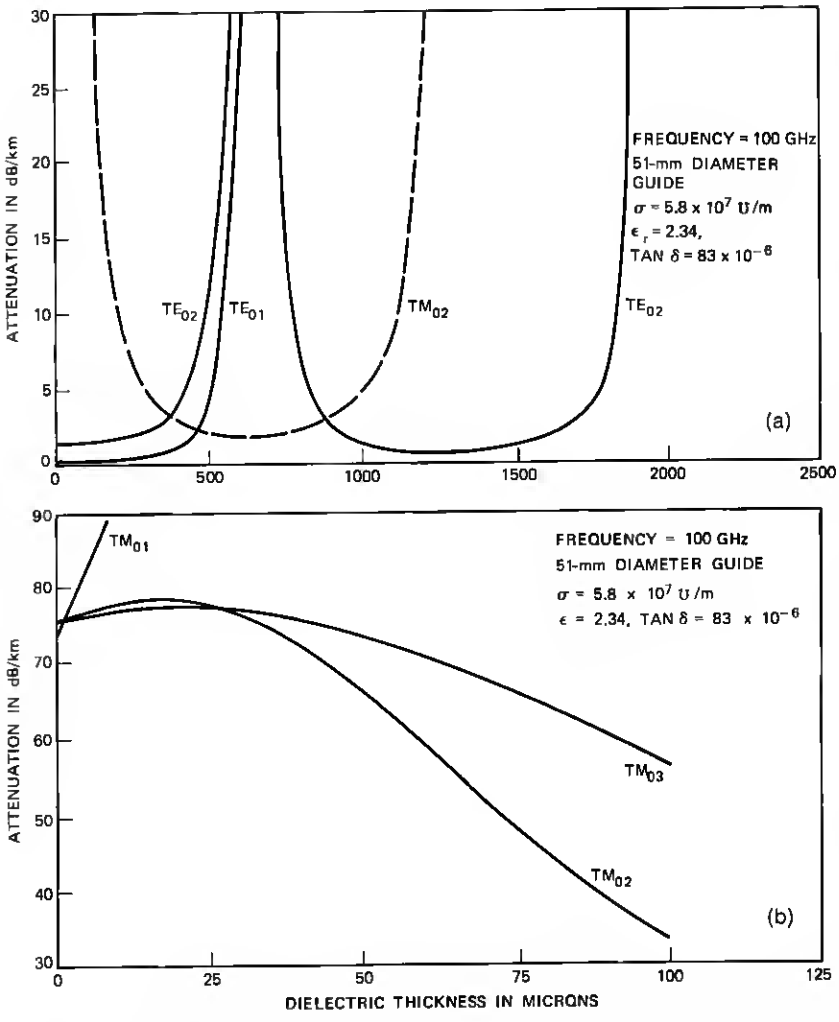

Fig. 5—Heat loss vs lining thickness for (a) the TE_{on} and TM_{on} modes; induced current method and (b) the TM_{on} modes; induced current method.

changes in the quarter-wavelength lining-thickness region. Figures 3 and 4 also furnish a good comparison of the exact solution (the curves shown in Figs. 3 and 4) for the eigenvalues and the "wall impedance" solution (the O's shown in the figures at selected points). The agreement is quite good with observed errors of approximately 2 percent or smaller for the cases shown.

In Figs. 5 and 6, the behavior of the total heat loss for some typical normal modes of DLG versus lining thickness is shown. We see that the TE_{on} modes are low loss for o, $\lambda/2$, λ, $\cdots$ thick linings while the TM_{on} modes exhibit low loss for $\lambda/4$, $3\lambda/4$, $\cdots$ thick linings.[5] The normal-mode heat loss exhibits the same periodic behavior vs lining thickness as the eigenvalues. The TE_{01} loss increases slowly with lining thickness for a thin lining; as the lining thickness approaches a quarter wavelength, the TE_{01} loss increases rapidly as the mode propagates as a surface wave.

The TE_{02} loss for a $\lambda/2$ lining is less than in unlined guide but still greater than that for the TE_{01} mode in unlined guide, as it is equivalent to the TE_{01} mode in a slightly smaller unlined guide.

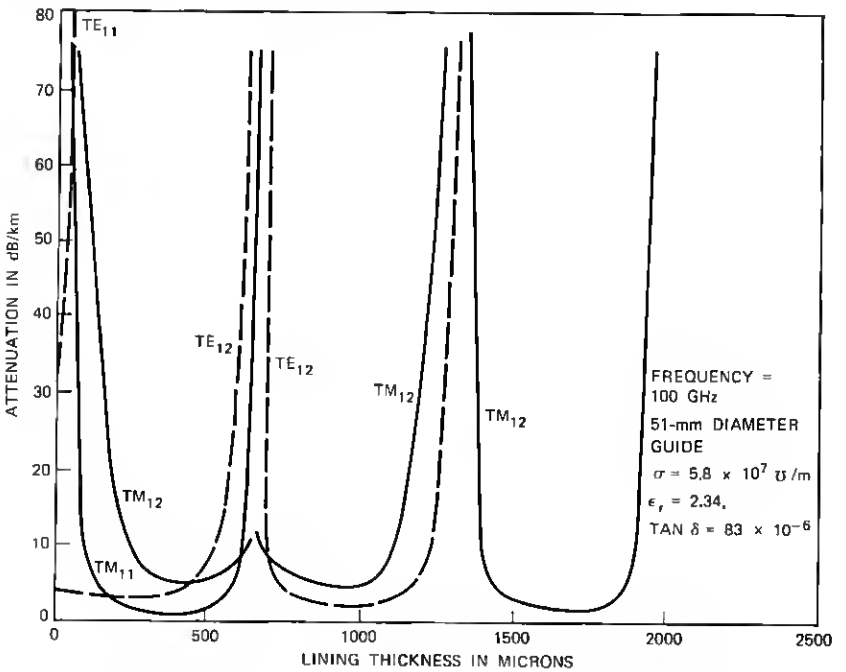

Fig. 6—Heat loss vs lining thickness for the TE_{1n} and TM_{1n} modes; induced current method.

The TM_{01} heat loss as shown in Fig. 5a increases rapidly for even very thin linings as expected for a surface wave mode. The TM_{on}, $n \neq 1$ (Figs. 5a and 5b), heat loss initially increases with lining thickness, and the initial slope of the loss curve agrees with the first-order perturbation theory of Unger,[3] but the loss then levels off (≈ 25 μm thick lining) and falls rapidly to a minimum for a quarter-wave lining (650 μm). The behavior of the TE_{1n} and TM_{1n} heat loss is similar to that of the TM_{on} and TE_{on} modes as shown in Fig. 6. The initial slope of the loss curves for the TE_{1n} and TM_{1n} modes versus thickness agrees with the perturbation theory predictions also, but from Figs. 5 and 6 it is obvious that the first-order perturbation theory is valid for predicting the normal-mode heat loss for only very thin linings (<20 μm). It is also quite clear that many modes (i.e., TE_{01}, TE_{02}, TE_{12}, TM_{11}, TM_{12}) as shown in Figs. 5 and 6 exhibit low heat loss (<5 dB/km for a 200-μm lining) in DLG.

Figure 7 is a comparison of the copper wall losses only for TE_{on} and TM_{on} modes as predicted by the induced current (the curves as shown) and the "wall impedance" method (the O's shown in the figure at

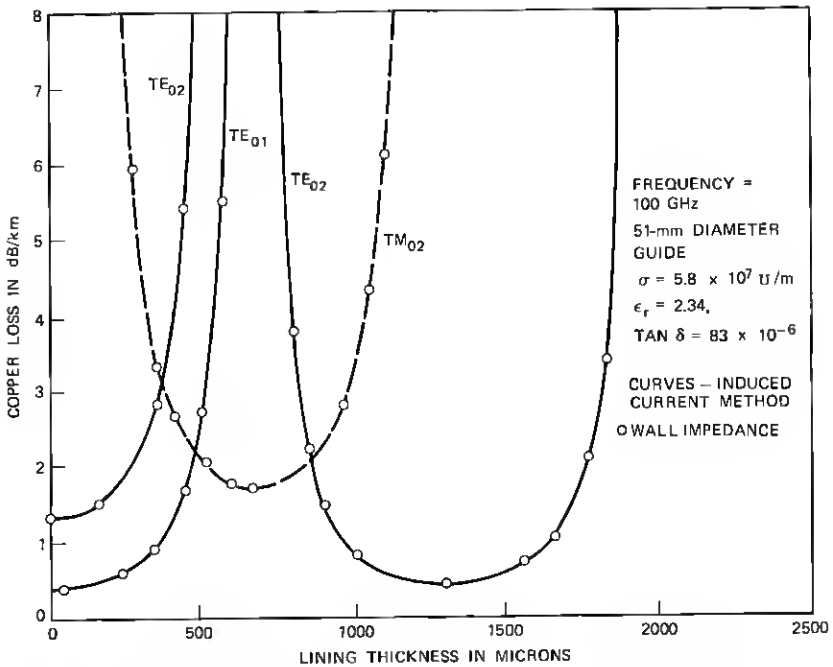

Fig. 7—Copper-loss comparison, wall impedance vs induced current method for the TE_{on} and TM_{on} modes.

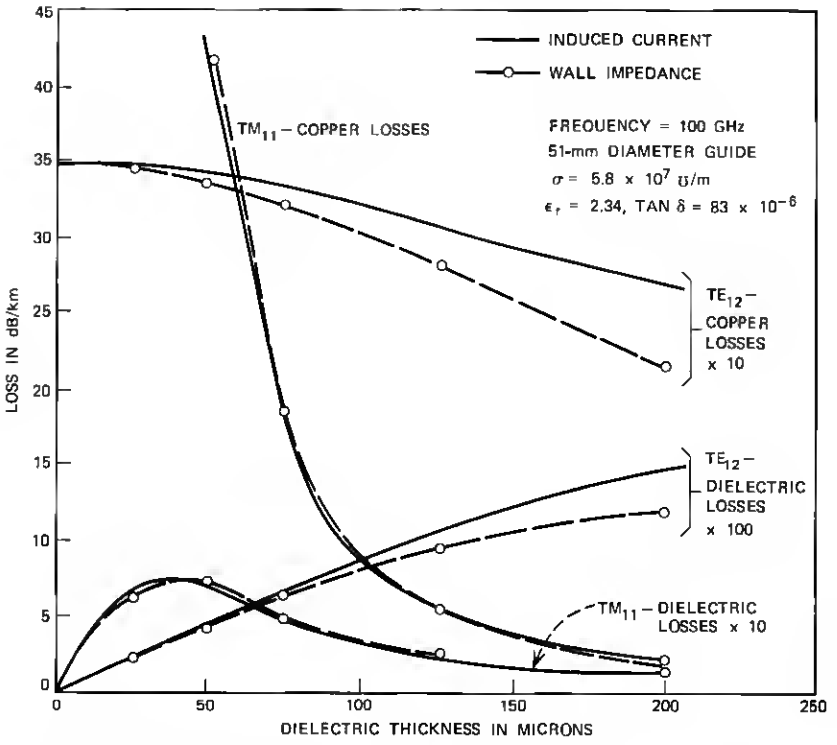

Fig. 8—Copper-loss comparison, wall impedance vs induced current method for the TE_{12} and TM_{11} modes.

selected points). The two methods are in excellent agreement over the range of thickness shown. Even in the regions where the losses are changing rapidly, the error is only on the order of 5 percent. The dielectric losses (not shown) are much smaller than the copper losses, but they also agreed to within 5 percent for the two methods.

Figure 8 is a comparison of the copper wall losses and dielectric losses predicted by the induced-current and wall-impedance methods for the TE_{12} and TM_{11} modes. The two methods differ by approximately 3 percent or less for the TM_{11} mode, but the TE_{12} difference is on the order of 10 to 20 percent for a 150 to 200-μm lining. The reason for this difference lies in the determination of the boundary conditions Z_z and Z_ϕ in (7). The approximate values of Z_z and Z_ϕ were obtained by use of a plane wave analysis as in Section III. This assumes a mode may be represented in the region local to the walls of the guide by a superposition of suitably polarized plane waves propagating in the

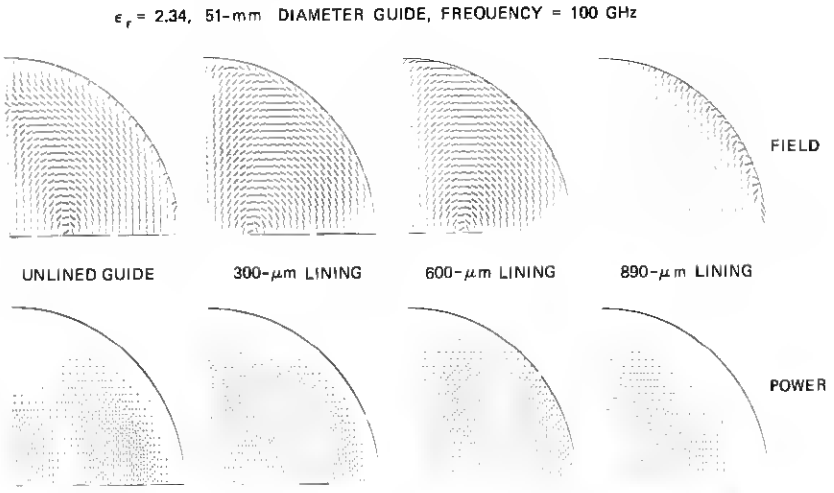

Fig. 9—TE_{12} electric field lines and power density vs lining thickness.

plane defined by the normal vector to the waveguide wall and the waveguide axis. This assumption is valid only for the circularly symmetric modes and leads to an error in the estimated boundary conditions (Z_z and Z_ϕ) for all other modes. The magnitude of the error is proportional to lining thickness to first order and has a greater effect on the loss of

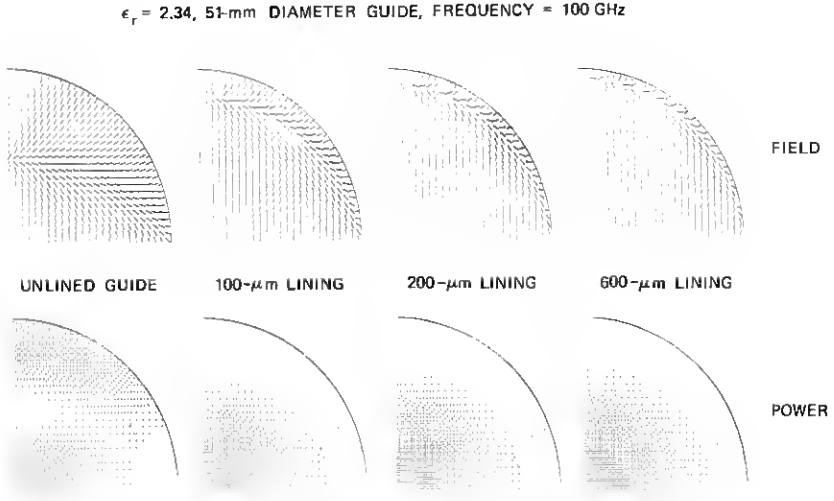

Fig. 10—TM_{11} electric field lines and power density vs lining thickness.

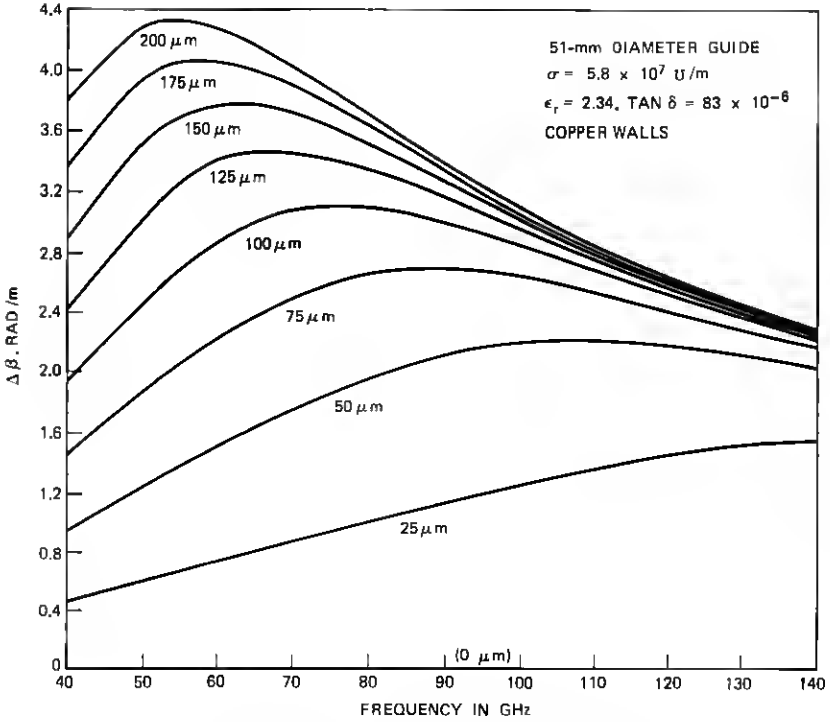

Fig. 11—TM_{11} $\Delta\beta$ vs frequency, wall-impedance model.

the TE_{pn} modes ($n \neq 1$), as they have a much lower loss than the TM_{pn} modes for thin linings.

Figures 9 and 10 are plots of the electric field lines and power distribution over a quadrant of the guide cross section for the TE_{12} and TM_{11} modes in the *free-space region* of the guide for various lining thicknesses at 100 GHz.

It can be seen that the lining drastically alters the field lines and energy distribution from those in copper waveguide. We also see that the low-loss regions of Fig. 6 are consistent with the energy distributions shown in Figs. 9 and 10 (as they correspond to the cases in Figs. 9 and 10 where the energy at the free-space dielectric interface is quite low). The TE_{12} energy density also changes much more slowly with lining thickness than does that for the TM_{11} mode as expected from the eigenvalue plots of Fig. 4. Note that the TM_{11} field lines and energy density change little over a 100- to 600-μm range of lining thickness. There would be a marked change for a lining thicker than 600 μm, as

the TM_{11} mode then assumes a surface wave behavior. The energy density distribution dependence on lining thickness was found to be similar for the circular symmetric TE_{on} and TM_{on} modes.

In the preceding discussion, we have considered the normal mode characteristics in DLG for unrealistically thick linings. (In Fig. 5, the TE_{01} heat loss is 21 dB/km at 100 GHz for the 600-μm thick polyethylene lining considered.) In the following paragraphs we will present some data for more representative lining thickness over a typical frequency band (40 to 110 GHz).

It is well known that a dielectric lining is required to break the degeneracy between the TE_{01} and TM_{11} modes in unlined guide. In Fig. 11, $\Delta\beta_{TM_{11}}$ is plotted for several lining thicknesses versus frequency. We see that for a lining thickness of greater than 150 μm the increase in $\Delta\beta$ is relatively small over the frequency range 70 to 110 GHz. We also note that $\Delta\beta$ is approximately inversely proportional to frequency for frequencies greater than 60 GHz for a 200-μm lining.

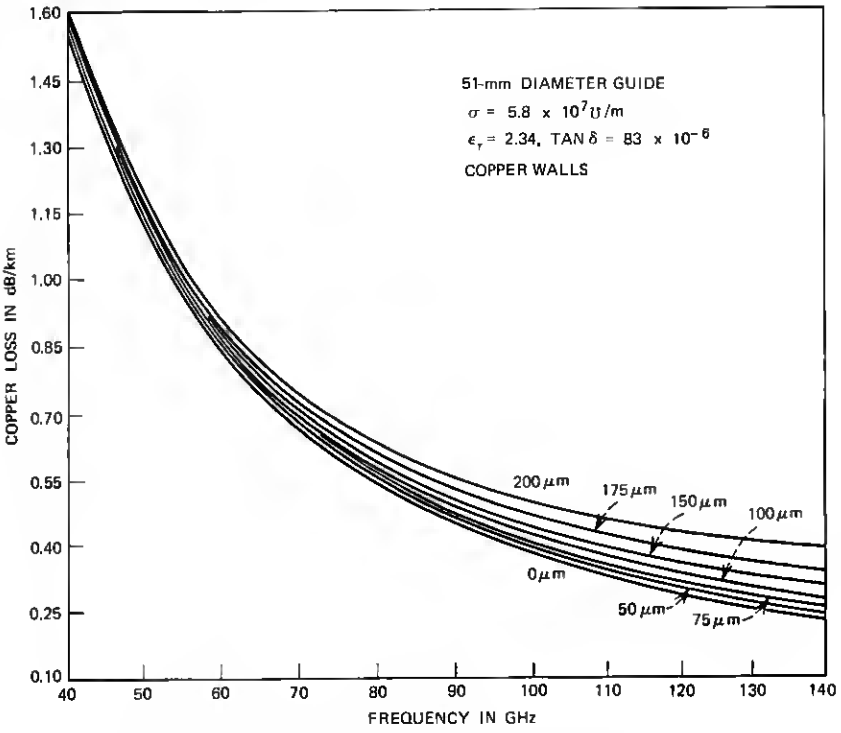

Fig. 12—TE_{01} copper loss vs frequency; wall-impedance model.

Conversely, in Figs. 12 and 13 it can be seen that a lining of 200 μm increases the TE_{01} copper loss by 0.12 dB/km at 110 GHz. The dielectric loss is negligible ($\approx$0.01 dB/km) for a 200-μm or thinner lining with a tan δ of 83 $\times$ 10^{-6}. On the other hand, the same liner with a tan δ of 10^{-3} would have a significant (0.12 dB/km) dielectric loss at 110 GHz. The preceding indicates a polyethylene liner with a thickness of 100 to 200 μm, and a tan $\delta < 10^{-4}$ is suitable for a transmission system using 51-mm diameter guide. A more precise determination of the optimal lining thickness is beyond the scope of this paper, as it depends in a complex fashion on the geometrical aberrations of the guide *in situ*.

Figures 14 through 16 are $\Delta\beta$ plots for several TE and TM modes over the 40- to 110-GHz band in 51-mm guide for 0, 100, and 200 μm polyethylene linings. The TE_{on} and $TE_{pn}(n > 1)$ mode $\Delta\beta$'s are quite close to the unlined guide $\Delta\beta$'s for a 200-μm lining and are essentially inversely proportional to frequency. The TM_{pn} mode $\Delta\beta$'s are strongly dependent on lining thickness for linings of 100 μm or less and essentially little changed for linings greater than 200 μm. The TM_{pn} mode

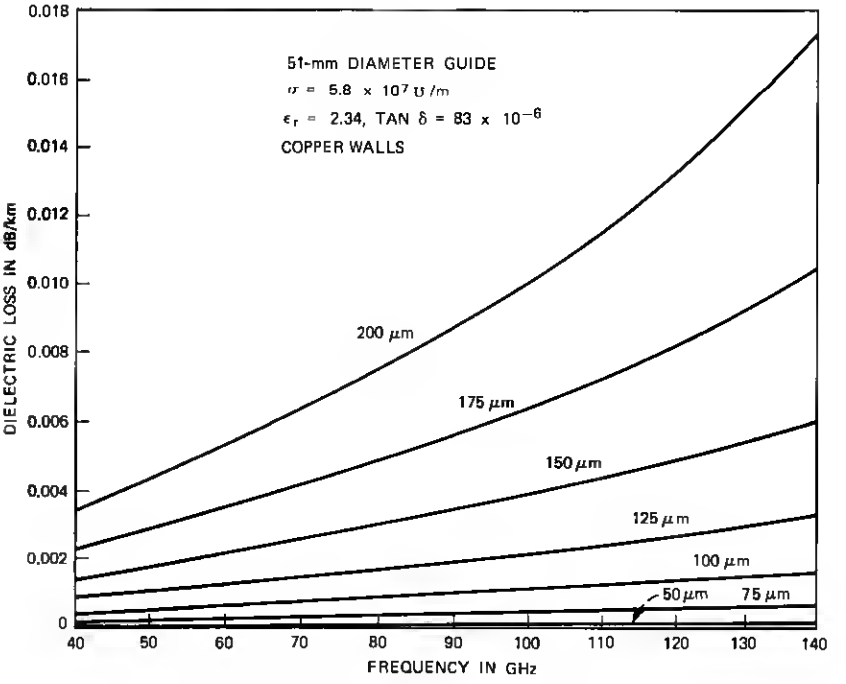

Fig. 13—TE_{01} dielectric losses vs frequency; wall-impedance model.

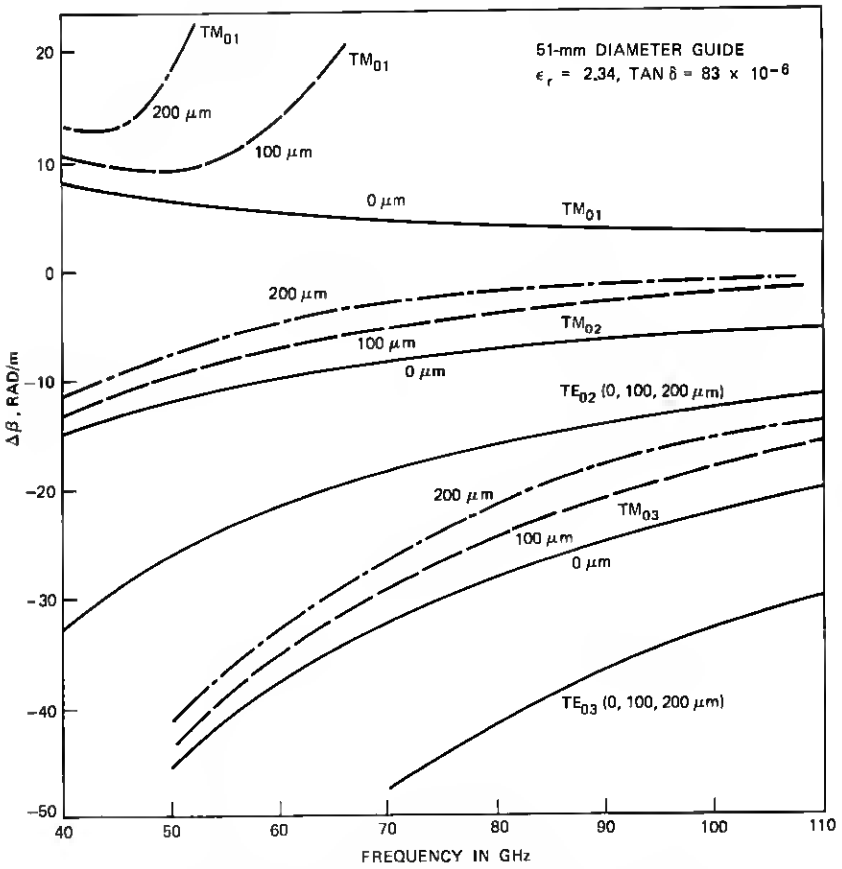

Fig. 14—TE_{on} and TM_{on} $\Delta\beta$ vs frequency; wall-impedance model.

$\Delta\beta$'s shown exhibit the $1/f$-type frequency dependence for a 200-μm lining for frequencies > 90 GHz. It should he noted that the TM_{21} mode has a very low $\Delta\beta$ for a 200-μm lining which necessitates the avoidance of long mechanical wavelength elliptical distortions over the guide cross section.

The TE_{p1} $\Delta\beta$'s are strongly dependent on lining thickness over the entire 40- to 110-GHz hand, and their hehavior is quite different from that of the other modes. This is due to the surface wave character of these modes. As a consequence of this, the TE_{p1} modes having eigenvalues >3.83171 (the TE_{01} eigenvalue in unlined guide) may become degenerate with the TE_{01} mode at selected frequencies within the hand of interest as shown in Fig. 17. The TE_{31} mode goes through a degener-

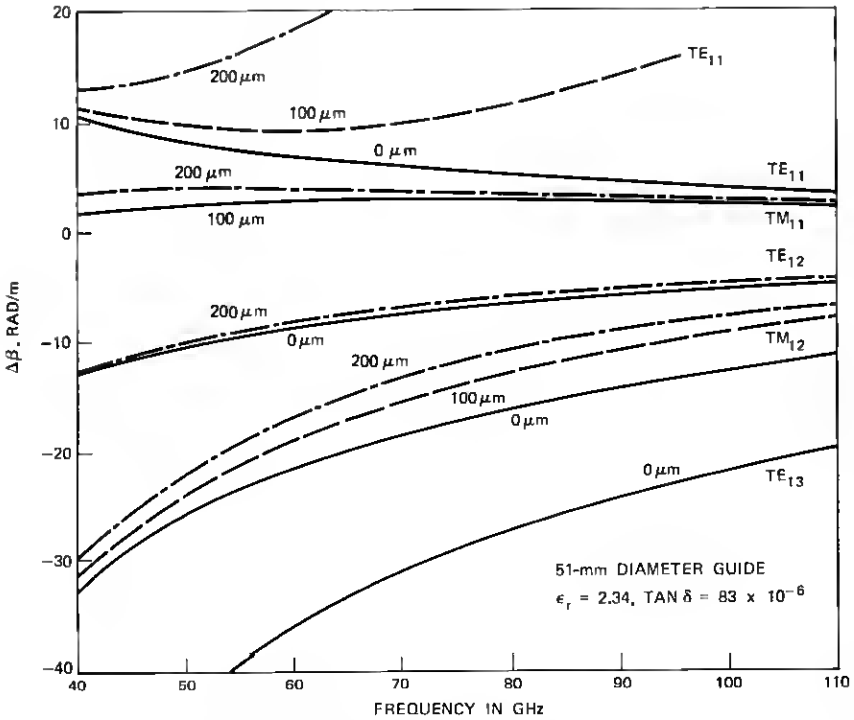

Fig. 15—TE_{1n} and TM_{1n} $\Delta\beta$ vs frequency; wall-impedance model.

acy at a frequency <40 GHz, while the TE_{21} and TE_{11} modes are never degenerate.

In Figs. 18 through 23, the heat loss of several normal modes is plotted for a 0-, 100-, and 200-μm polyethylene lining in 51-mm guide over the 40- to 110-GHz band. The characteristics may be summarized as:

(*i*) The TM_{pn} (except for the TM_{01} mode) heat loss initially increases with frequency, levels off, and then decreases by an order of magnitude for a 200-μm lining from 40 to 110 GHz. The presence of the lining substantially reduces the heat loss at 110 GHz. The losses are as low as 3 dB/km at 110 GHz.

(*ii*) The TE_{on} losses decrease with frequency, but not in the $f^{-\frac{1}{2}}$ fashion as in unlined guide. The presence of a lining leads to a frequency-dependent increase in heat loss over the 40- to 100-GHz band; approximately 5 percent and 30 percent for

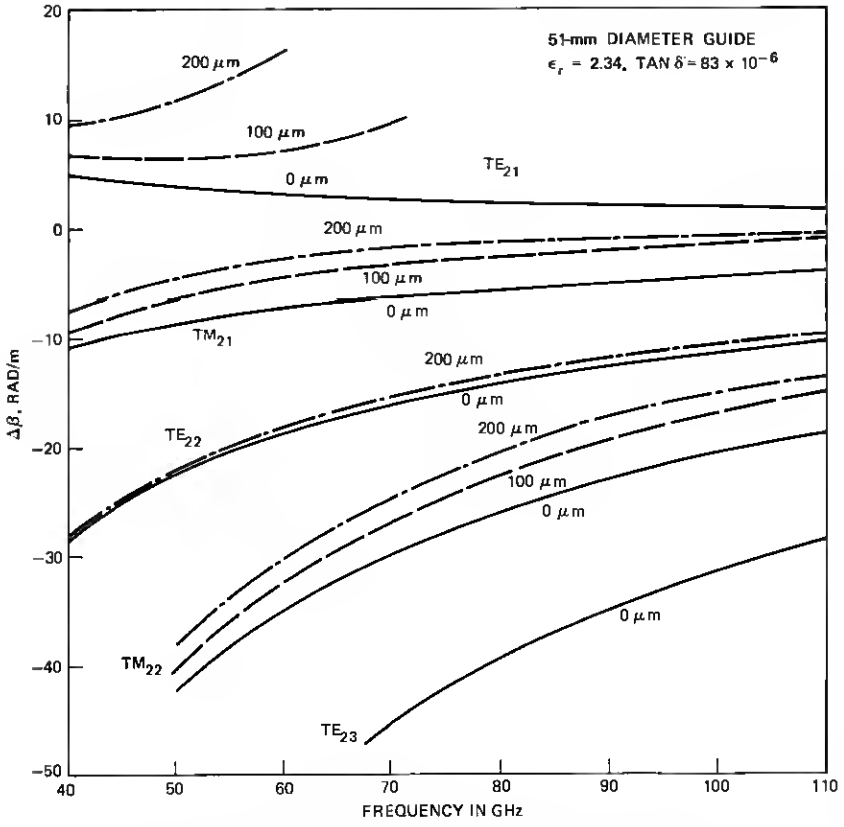

Fig. 16—TE_{2n} and TM_{2n} $\Delta\beta$ vs frequency; wall-impedance method.

the TE_{01} mode at 40 and 110 GHz, respectively, for a 200-μm lining.

(*iii*) The TE_{p1} and TM_{01} heat loss is quite high (>100 dB/km) for even thin linings, as these are surface-wave-type modes.

(*iv*) The TE_{pn} ($n \neq 1$) heat loss is low (<10 dB/km), and the presence of the lining actually reduces the heat loss over much of the 40- to 110-GHz range.

(*v*) The heat loss is substantially different from that predicted by the simple perturbation[3] theory for thin linings (for linings >10 μm) except in the case of the TE_{on} modes.

The normal mode characteristics, and in particular the low loss of the TM_{pn} modes, discussed in the previous paragraphs (Figs. 3 through 23) can be easily understood on recognizing that the lower-order modes

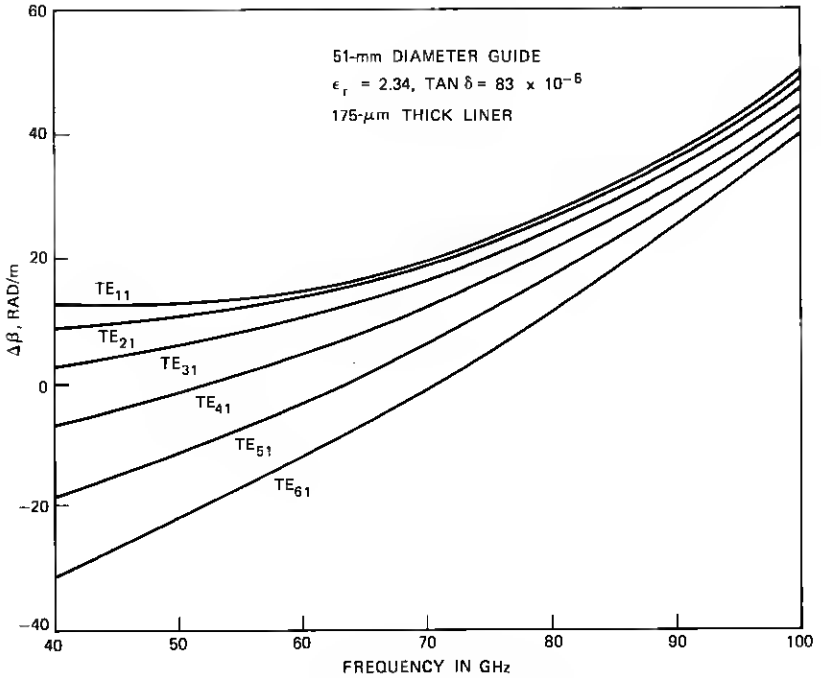

Fig. 17—TE_{n1} $\Delta\beta$ vs frequency; exact solution.

have a plane-wave-type field structure. The electric field of the plane waves may be polarized perpendicular (TE_{on} modes) to or parallel (TM_{on} modes) to the plane of incidence as shown in Fig. 24. A TE_{pn} or TM_{pn} mode (for $p \neq 0$) is necessarily a superposition of both polarizations.

In examining the interaction of these plane waves with the walls of the guide, it is helpful to consider the transmission line equivalent structures of Fig. 24. The transmission line parameters (characteristic impedance Z_c and propagation constant k_r in the radial direction) are dependent on the polarization. In the empty region of the waveguide they are given by:

Perpendicular Polarization TE_{on} Modes	Parallel Polarization TM_{on} Modes
$k_r = k_n/a$	$k_r = k_n/a$
$Z_c = \eta \dfrac{ka}{k_n}$	$Z_c = \eta \dfrac{k_n}{ka}$

(10)

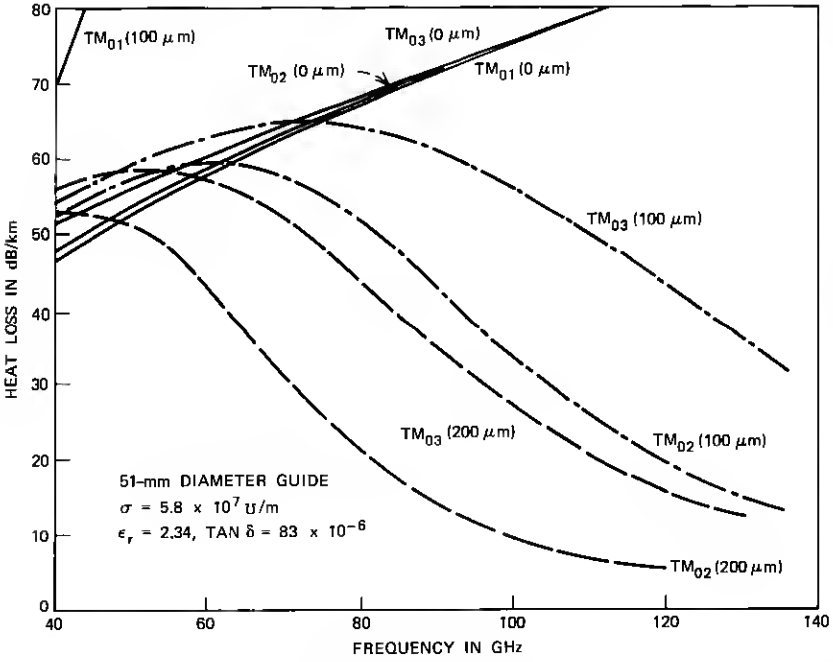

Fig. 18—TM_{on} heat loss vs frequency; wall-impedance model.

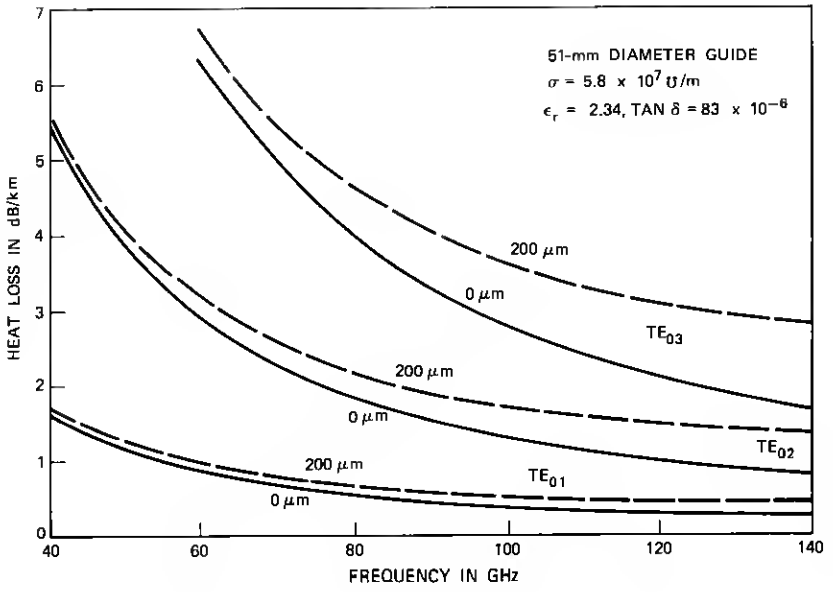

Fig. 19—TE_{on} heat loss vs frequency; wall-impedance model.

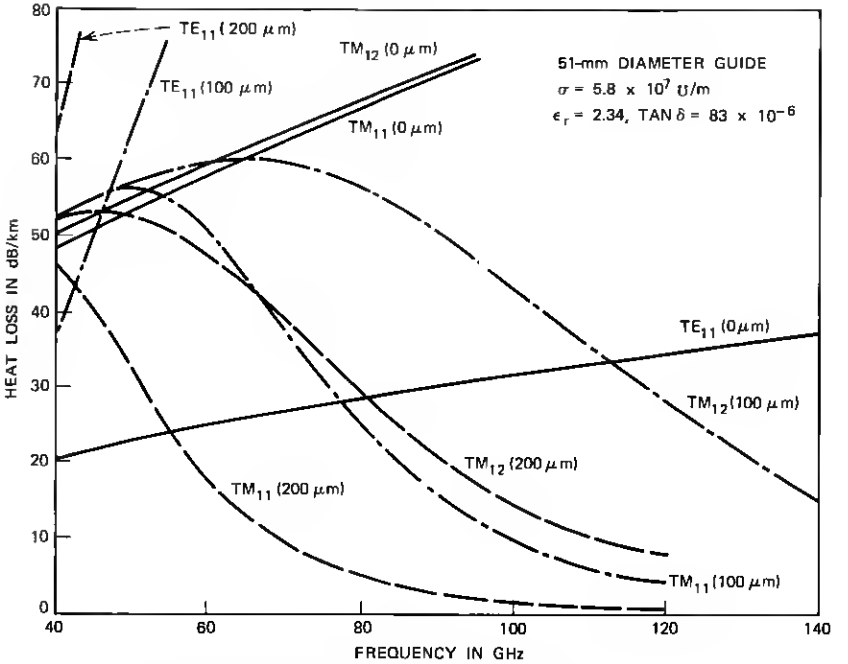

Fig. 20—TE_{11} and TM_{1n} heat loss vs frequency; wall-impedance model.

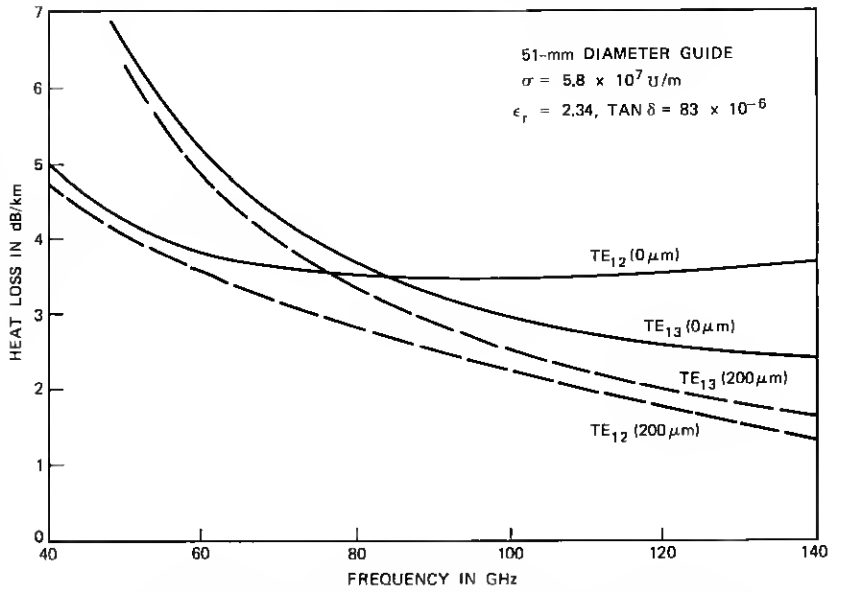

Fig. 21—TE_{12} and TE_{13} heat loss vs frequency; wall-impedance model.

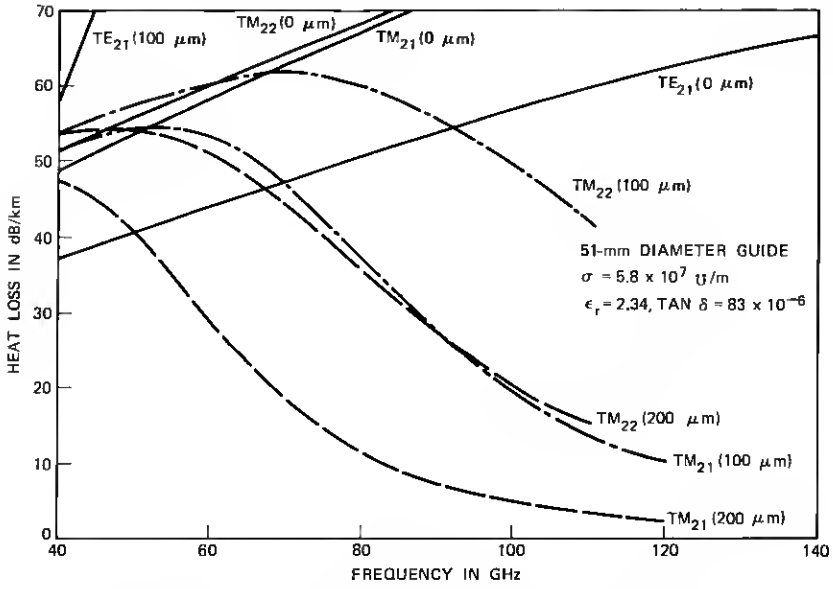

Fig. 22—TE_{21} and TM_{2n} heat loss vs frequency; wall-impedance model.

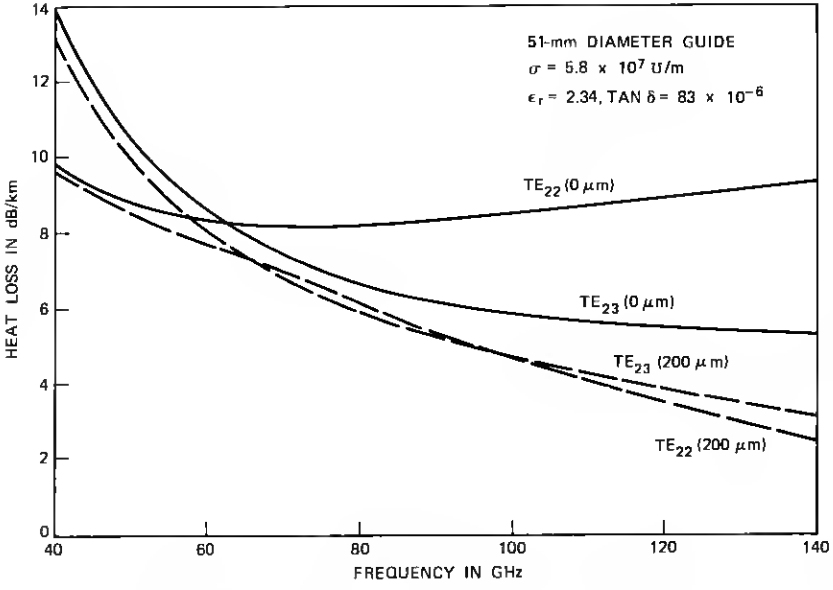

Fig. 23—TE_{22} and TE_{23} heat loss vs frequency; wall-impedance model.

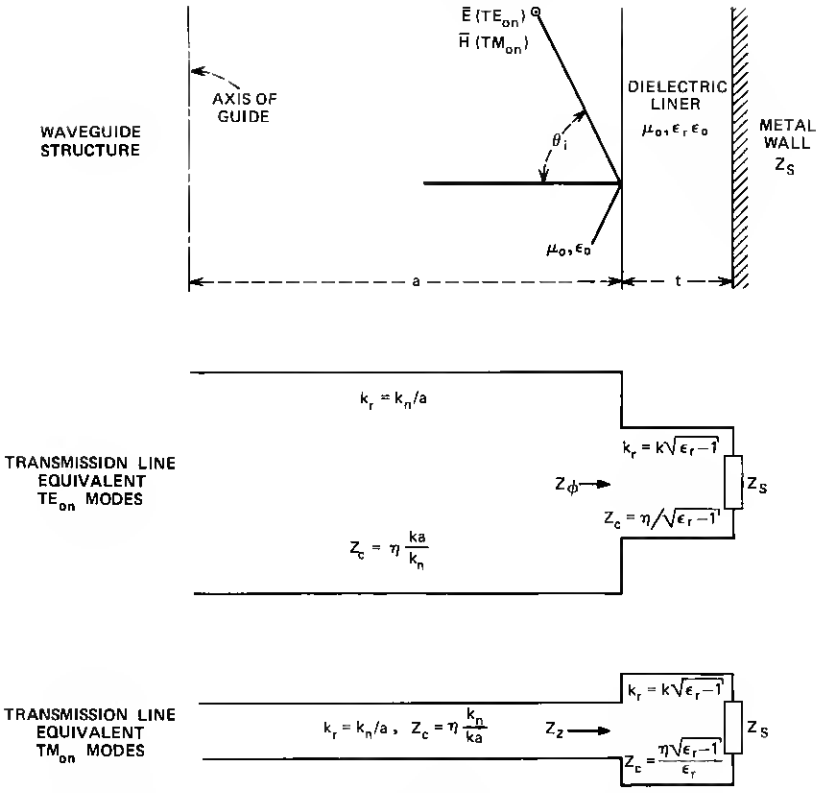

Fig. 24—Equivalent transmission line structures for the TE$_{on}$ and TM$_{on}$ modes.

where η is the impedance of free space, k_n the eigenvalue for the mode of interest, a the guide radius, and k the free-space propagation constant. In the dielectric region we have for the near grazing incidence ($\theta_i \cong 90°$) case:

Perpendicular Polarization TE$_{on}$ Modes	Parallel Polarization TM$_{on}$ Modes
$k_r \cong k\sqrt{\epsilon_r - 1}$	$k_r \cong k\sqrt{\epsilon_r - 1}$
$Z_c \cong \eta/\sqrt{\epsilon_r - 1}$	$Z_c \cong \eta\sqrt{\epsilon_r - 1}/\epsilon_r$

(11)

The single-layer case may be generalized to the multilayer case by simply adding the equivalent transmission line sections. The copper walls of the structure have a skin-effect surface impedance on tbe order of $0.05 + j\,0.05$ to $0.1 + j\,0.1$ ohms at 40 and 110 GHz, respectively,

for hoth polarizations. On transforming these impedances in the normal way through a 200-μm polyethylene liner with equivalent transmission line parameters as given hy (11), we ohtain the wall impedances Z_z and Z_ϕ which are seen at the dielectric free-space interface. These are on the order of $0.05 + j\,50$ to $0.1 + j\,200$ ohms. On the other hand, the characteristic impedances as given in (10) for the lower-order modes of most interest in the empty region of the guide are on the order of 10 to 80 ohms for parallel polarization (TM_{on} modes), while the perpendicular polarization (TE_{on}) characteristic impedances are on the order of 1000 to 10,000 ohms.

The reflection coefficients of the dielectric-clad copper wall for the equivalent transmission line structures in Fig. 24 are a function of Z_z/Z_c or Z_ϕ/Z_c. The propagation constant h_n or attenuation constant α for the mode of interest is related to the phase or amplitude of the appropriate reflection coefficient, respectively. In unlined copper guide, hoth of these ratios (Z_z/Z_c and Z_ϕ/Z_c) are $\ll 1$. For the TM_{on} modes in DLG, $|Z_z|$ is on the order of or much greater than Z_c, and thus these modes are drastically changed from their copper guide equivalents. This is shown hy the large changes in $\Delta\beta$ for these modes and the drastic reduction in the heat loss. On the other hand, $|Z_\phi|$ is much less than Z_c for the TE_{on} modes, and hence the $\Delta\beta$ and heat loss of these modes is little changed from that in copper guide. The TE_{pn} modes ($n \neq 1$, $p \neq 0$) have a TE_{on}-like field structure in the region of the wall in copper guide and thus are little affected hy the lining. The TM_{pn} and TE_{p1} modes have a TM_{on}-like field structure in the wall region in copper guide, and they are drastically altered hy the presence of a lining as we have ohserved.

IV. SYSTEM IMPLICATIONS

In the preceding sections, we have seen that the TM_{11} and TE_{12} modes have very low heat losses ($\lesssim 3$ dB/km) at 110 GHz. This low heat loss leads to a reduction in route hend losses as can he seen in the following. Unger[3] shows that the TE_{01} mode undergoes added losses in a route hend due to two different effects. The first effect, called mode conversion loss, arises from the fact that a portion of the TE_{01} energy is converted into other modes (predominantly TM_{11} and TE_{12} in DLG) in the hend and is not reconverted back to the TE_{01} mode hut instead emerges from the hend as a spurious mode.

The second loss mechanism, defined as the added heat loss, is associated with the energy initially converted from the TE_{01} mode to the TE_{12} or TM_{11} mode and then reconverted hack to the TE_{01} mode as

the hend is traversed. Since this energy travels in the higher-loss TE_{12} and TM_{11} modes over a portion of the hend, it suffers additional attenuation over and ahove the TE_{01} heat loss in DLG. For a given mode, the mode conversion loss and added heat loss in a route hend of radius R and total bend length L, with a taper length ℓ (the radius of curvature is assumed to have a linear taper of 0 to R from 0 to ℓ and R to 0 for $L - \ell$ to L), is given by

$$\begin{aligned} L_{\text{RB–AH}}\ (\text{added heat loss}) &= \frac{L - \frac{3}{4}\ell}{R^2}\,\frac{C^2}{\Delta\beta_n^2}\,\Delta\alpha_n \\ L_{\text{RB–MC}}\ (\text{mode conversion loss}) &= \frac{4}{(R\ell)^2}\,\frac{C^2}{\Delta\beta_n^4}. \end{aligned} \tag{12}$$

Here C is the normalized coupling coefficient[4] due to curvature of the guide axis, and the other parameters are as previously defined. In Figs. 25 and 26, the total added TE_{01} loss, due to the route bend, as

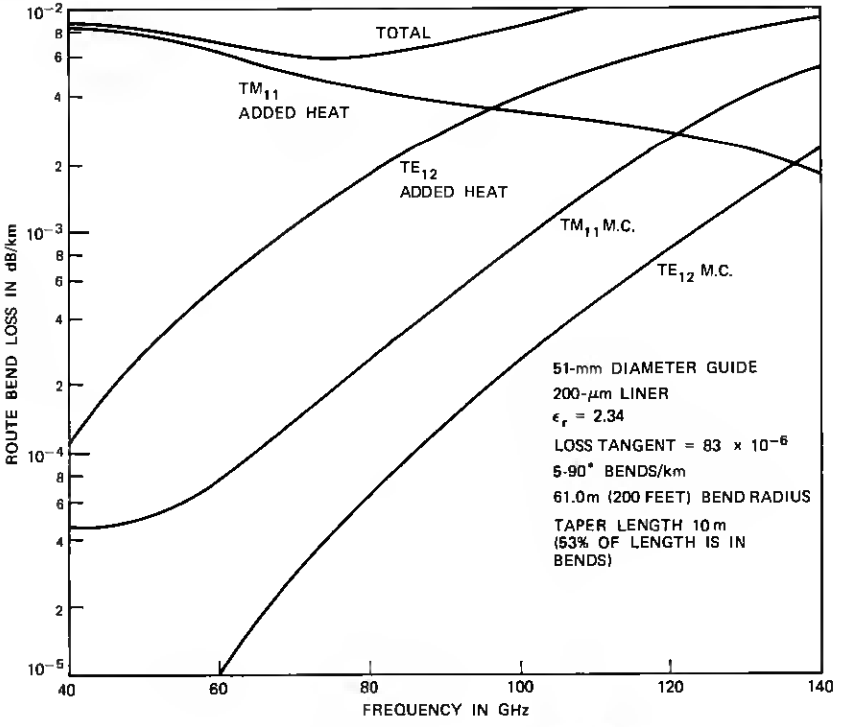

Fig. 25—Theoretical route bend losses.

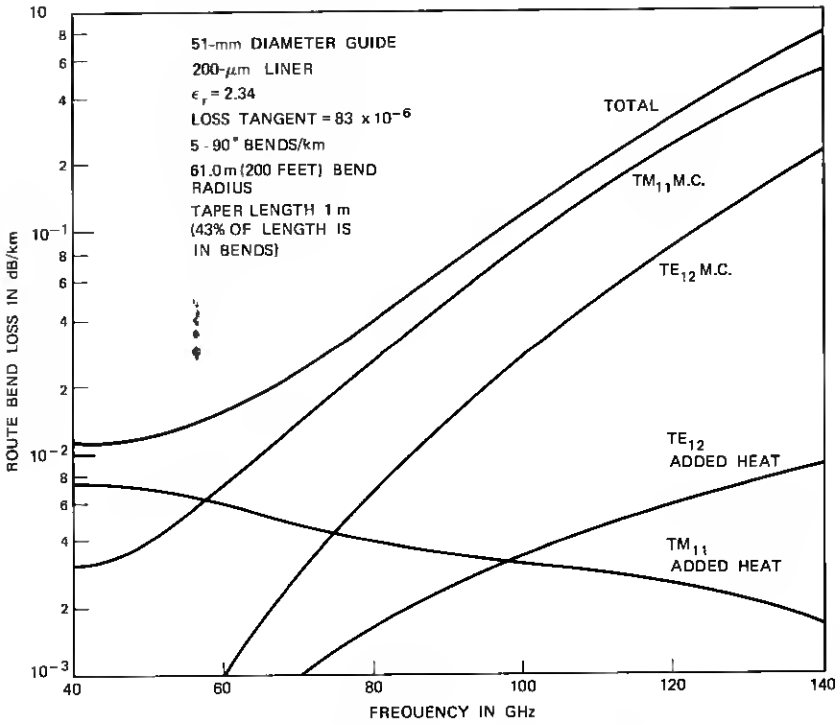

Fig. 26—Theoretical route bend losses.

well as the individual components comprising it is plotted for some idealized routes comprised of five 90-degree bends with a constant radius of curvature (61 m) and linear tapers of 1 or 10 m in length in DLG over a length of 1 km.

From Fig. 26, it is obvious that the mode conversion losses are far more significant then the added heat loss in route bends with a short taper (or zero) length. On the other hand, for a reasonable taper length (10 m), the mode conversion losses are significantly lower than the added heat loss arising from coupling to the TM_{11} and TE_{12} modes. The linear taper is probably a reasonable approximation to that expected in practice as the radius of curvature will change in a smooth fashion as the waveguide progresses from a straight run into a curve.

The added heat loss is substantially reduced by the presence of the lining due to the great reduction in the TM_{11} heat loss. For example, at 110 GHz the TM_{11} mode yields an added heat loss for the route bends of Fig. 25 of approximately 0.005 dB/km. If the TM_{11} mode

heat loss had followed the perturbation[3] theory prediction, the added heat loss for the same route bend would be ≈ 0.250 dB/km.

V. CONCLUSION

We have discussed the basic propagation characteristics of the normal modes of dielectric-lined overmoded circular waveguide. Some of the results obtained differ in surprising fashion from those predicted by the perturbation theory of Unger.[3] The most significant result is the low heat loss of the TM_{1n} modes at the upper end of the 40- to 110-GHz band discussed. This effect greatly reduces the added heat loss for the TE_{01} mode in route bends over this part of the frequency spectrum.

A simple physical explanation based on an equivalent transmission line problem derived from an analogous plane-wave problem was advanced to support the results contained here. An experimental investigation of the decreasing TM_{11} heat loss[6] vs frequency has been completed, and the data confirm the trends predicted herein.

VI. ACKNOWLEDGMENT

The authors are indebted to W. DeLang for his perspicacity and thoroughness in carrying out the numerical computations.

APPENDIX A

Exact Formulation

The waveguide structure under consideration is shown in Fig. 1 of the main text of this paper. The notation used conforms with that of Unger.[4] Much of the following is similar to that contained in Unger[3,4] but is repeated here for reasons of continuity and completeness.

The fields in the guide can be derived from two suitable scalar wave functions composed of suitable products of trigonometric and Bessel functions.

$$\begin{aligned} T_n &= N_n J_p(\chi_n r) \sin p\phi \\ T'_n &= N_n J_p(\chi_n r) \cos p\phi \end{aligned} \qquad 0 < r < a \tag{13}$$

$$\begin{aligned} T_n &= N_n \frac{\chi_n^2}{\chi_n^{e2}} J_p(k_n) \frac{Z_{pn}(\chi_n^e r)}{Z_{pn}(k_n^e)} \sin p\phi \\ T'_n &= N_n \frac{\chi_n^2}{\chi_n^{e2}} J_p(k_n) \frac{Z_{pn}(\chi_n^e r)}{Z_{pn}(k_n^e)} \cos p\phi \end{aligned} \qquad a < r < b \tag{14}$$

where

$$Z_{pn}(\chi_n^e r) = H_p^{(2)}(\chi_n^e r) - cH_p^{(1)}(\chi_n^e r)$$
$$Z_{pn}(\chi_n^e r) = H_p^{(2)}(\chi_n^e r) - c'H_p^{(1)}(\chi_n^e r).$$

Z'_{pn} and Z'_{pn} are the derivatives of the above expressions with respect to the entire argument. The constants c and c' will he defined later. The T functions satisfy tbe wave equation

$$\nabla_t^2 T = \frac{1}{r}\left[\frac{\partial}{\partial r}\left(r\frac{\partial T}{\partial r}\right) + \frac{\partial}{\partial \phi}\left(\frac{1}{r}\frac{\partial T}{\partial \phi}\right)\right] = -\chi^2 T \tag{15}$$

wbere χ^2 is given hy χ_n^2 or χ_n^{e2} for $0 < r < a$ or $a < r < b$ respectively, and ∇_t^2 is the transverse Laplacian operator.

The fields in the guide may be derived from the scalar wave functions as in Unger[4]

$$E_r = \sum_n V_n\left[\frac{\partial T_n}{\partial r} + d_n\frac{\partial T'_n}{r\partial\phi}\right]$$
$$E_\phi = \sum_n V_n\left[\frac{\partial T_n}{r\partial\phi} - d_n\frac{\partial T'_n}{\partial r}\right]$$
$$H_r = -\sum_n I_n\left[\frac{\partial T_n}{r\partial\phi} - d_n\frac{h_n^2}{k^2\epsilon}\frac{\partial T'_n}{\partial r}\right]\epsilon$$
$$H_\phi = \sum I_n\left[\frac{\partial T_n}{\partial r} + d_n\frac{h_n^2}{k^2\epsilon}\frac{\partial T'_n}{r\partial\phi}\right]\epsilon \tag{16}$$

$$H_z = j\omega\epsilon\epsilon_0\sum_n V_n d_n\frac{\chi^2}{k^2}T'_n$$

$$E_z = j\omega\mu_0\sum_n I_n\epsilon\frac{\chi^2}{k^2}T_n \tag{17}$$

where μ_0 and ϵ_0 are the permeahility and permittivity of free-space, respectively, ϵ is the relative permittivity (1 for $0 < r < a$, ϵ_r for $a < r < b$) over the guide cross section, $k = \omega\sqrt{\mu_0\epsilon_0\epsilon}$ is the intrinsic plane-wave propagation constant in the various regions of the guide. Here, ϵ, k, and χ have constant but different values over the guide cross section as may the separation constant d_n. A mode for the structure consists of one term in the series given in (16) and (17). For a given modal field distribution, the individual V_n and I_n's in (16) and (17) represent a *single* forward or backward traveling wave, and tbey are related to each other by tbe modal impedance Z_n

$$\frac{V_n}{I_n} = Z_n = \frac{h_n}{\omega\epsilon_0}. \tag{18}$$

Imposition of the appropriate boundary conditions at $r = a$, and $r = b$ leads to a determination of d_n, c, c', χ_n, and χ_n^e on solution of a transcendental equation. From Unger[4] we have

$$c = \frac{H_p^{(2)}(\rho k_n^e)}{H_p^{(1)}(\rho k_n^e)} \tag{19}$$

$$c' = \frac{H_p^{(2)\prime}(\rho k_n^e)}{H_p^{(1)\prime}(\rho k_n^e)} \tag{20}$$

where the $'$ associated with the Bessel function denotes differentiation with respect to the entire argument. We also define ρ, k_n, and k_n^e

$$\rho = b/a \tag{21}$$

$$k_n = \chi_n a \tag{22}$$

$$k_n^e = \chi_n^e a. \tag{23}$$

We find d_n is constant over the guide cross section and is given by

$$\frac{1}{d_n} = \frac{k_n^2 k_n^{e2}}{pk^2a^2(\epsilon_r - 1)} [y_{pn}(k_n) - Y_{pn}(k_n^e)] \tag{24}$$

where

$$\begin{aligned} y_{pn} &= \frac{J_p'(k_n)}{k_n J_p(k_n)} \\ Y_{pn}(k_n^e) &= \frac{Z_{pn}'(k_n^e)}{k_n^e Z_{pn}(k_n^e)} \\ Y_{pn}(k_n^e) &= \frac{Z_{pn}'(k_n^e)}{k_n^e Z_{pn}(k_n^e)}. \end{aligned} \tag{25}$$

k_n and k_n^e are related by

$$\begin{aligned} k_n^2 &= (\omega^2 \epsilon_0 \mu_0 - h_n^2)a^2 \\ k_n^{e2} &= (\omega^2 \epsilon_r \epsilon_0 \mu_0 - h_n^2)a^2. \end{aligned} \tag{26}$$

The individual modes may be determined by solution of the eigenvalue equation:

$$[y_{pn}(k_n) - Y_{pn}(k_n^e)] \cdot [y_{pn}(k_n) - \epsilon_r Y_{pn}(k_n^e)] = p^2(\epsilon_r - 1)^2 \frac{h_n^2 k^2 a^4}{k_n^4 k_n^{e4}} \tag{27}$$

for quasi TE_{pn}, TM_{pn} modes, $p \neq 0$. For circular electric waves ($p = 0$), the eigenvalue equation is

$$[y_{on}(k_n) - Y_{on}(k_n^e)] = 0. \tag{28}$$

For circular magnetic waves (TM_{0n}) we have

$$[y_{on}(k_n) - \epsilon_r Y_{on}(k_n^e)] = 0. \tag{28a}$$

The constant N_n is given by imposing an ortho-normalization criterion on the transverse fields given in (16). This condition is

$$\frac{1}{V_n I_m} \int\int \bar{E}_n \times \bar{H}_m \cdot d\bar{s} = \begin{cases} 1 & n = m \\ 0 & n \neq m. \end{cases}$$

On evaluation of this integral, we find that N_n is exactly given by

$$\begin{aligned} \frac{\pi}{2} N_n^2 k_n^2 J_p^2(k_n) \Bigg\{ & \left(1 + \frac{d_n^2 h_n^2}{k^2}\right)\left(1 - \frac{p^2}{k_n^2} + k_n^2 y_{pn}^2 + 2y_{pn}\right) \\ & - 2d_n \frac{p}{k_n^2}\left[\left(1 + \frac{h_n^2}{k^2}\right) - \left(1 + \frac{h_n^2}{\epsilon_r k^2}\right)\frac{\epsilon_r k_n^4}{k_n^{e4}}\right] \\ & + \left(\frac{k_n}{k_n^e}\right)^2 \frac{d_n^2 h_n^2}{k^2}\left(p^2 \frac{Z_{pn}^2(\rho k_n^e)}{Z_{pn}^2(k_n^e)}\right)\left[1 - \frac{p^2}{\rho^2 k_n^{e2}}\right] \\ & - \left[1 - \frac{p^2}{k_n^{e2}} + k_n^{e2} Y_{pn}^2 + 2Y_{pn}\right] \\ & + \epsilon_r \left(\rho^2 \frac{Z_{pn}^{2\prime}(\rho k_n^e)}{Z_{pn}^2(k_n^e)} - \left[1 - \frac{p^2}{k_n^{e2}} + k_n^{e2} Y_{pn}^2 + 2Y_{pn}\right]\right)\Bigg\} = 1 \end{aligned} \tag{29}$$

for TE_{pn} or TM_{pn} modes, $p \neq 0$ and by

$$\begin{aligned} & \pi N_n^2 k_n^2 J_o^2(k_n) \frac{d_n^2 h_n^2}{k^2} \Bigg\{(1 + k_n^2 y_{on}^2 + 2y_{on}) \\ & \qquad + \left(\frac{k_n}{k_n^e}\right)^2 \left[\rho^2 \frac{Z_{on}^2(\rho k_n^e)}{Z_{on}^2(k_n^e)} - (1 + k_n^{e2} Y_{on}^2 + 2Y_{on})\right]\Bigg\} = 1 \end{aligned}$$

$$\begin{aligned} & \pi N_n^2 k_n^2 J_o^2(k_n) \Bigg\{(1 + k_n^2 y_{on}^2 + 2y_{on}) \\ & \qquad + \epsilon_r \left(\frac{k_n}{k_n^e}\right)^2 \left[\rho^2 \frac{Z_{on}'^2(\rho k_n^e)}{Z_{on}^2(k_n^e)} - (1 + k_n^{e2} Y_{on}^2 + 2Y_{on})\right]\Bigg\} = 1 \end{aligned}$$

for circular electric (TE_{0m}) and magnetic (TM_{0n}) modes, respectively. We shall use a subscript n when referring to TE_{pn} or TM_{pn} modes and a subsequent m for TE_{om} modes.

Solution of the appropriate eigenvalue equation (27) or (28) leads to a value for the propagation constant (h_m or h_n) which is pure real as we have assumed a lossless dielectric-lined guide in the above analy-

sis. For an actual guide, h_n and h_m have a small imaginary part which we call the attenuation constant (α_{om} or α_{pn}) for the mode in question. The loss is due to currents flowing in the metal walls of the guide and the lossy dielectric.

The heat loss or attenuation constant (α) due to currents flowing in the metal walls of the structure is given by

$$\alpha = \frac{1}{2}\frac{P_L}{P_T}$$

where

$$P_L = \frac{1}{2}\int i\cdot i^* R_s\, dS = \frac{1}{2}\int_0^1 \int_0^{2\Pi} (H_z\cdot H_z^* + H_\phi\cdot H_\phi^*)\Big|_{r=b} R_s\, b\, d\phi\, dz,$$

i.e., power loss/unit length,

$$P_T = \frac{1}{2}\int E_t \times H_t^* ds = \frac{1}{2}\int E_t \times H_t\, dS = \tfrac{1}{2} V_n I_n,$$

i.e., the total average power flowing through the guide cross section for a given mode, and R_s is the surface resistance of the metal walls.

$$H_z(b) = j\frac{V_n d_n}{\omega\mu_0} N_n \chi_n^2 J_p(k_n)\frac{Z_{pn}(\rho k_n^e)}{Z_{pn}(k_n^e)}\cos p\phi$$

$$H_\phi(b) = I_n \epsilon_r N_n \frac{\chi_n^2}{\chi_n^{e2}}\left[\chi_n^e \frac{Z'_{pn}(\rho k_n^e)}{Z_{pn}(k_n^e)} - d_n \frac{h_n^2 p}{\omega^2\mu_0\epsilon_0\epsilon_r b}\frac{Z_{pn}(\rho k_n^e)}{Z_{pn}(k_n^e)}\right]\sin p\phi$$

noting $I_n = V_n/K_n$ where $K_n = h_n/\omega\epsilon_0$. We find

$$\alpha_{pn_{\text{copper}}} = \frac{\Pi}{2}\frac{h_n R_s}{\omega\epsilon_0}|N_n|^2\left(\frac{k_n}{k_n^e}\right)^4 J_p^2(k_n) b \times \left\{\left(\frac{\omega\epsilon_r\epsilon_0}{h_n}\right)^2\left|\chi_n^e\frac{Z'_{pn}(\rho k_n^e)}{Z_{pn}(k_n^e)} - \frac{d_n h_n^2 p}{\omega^2\mu_0\epsilon_0\epsilon_r b}\frac{Z_{pn}(\rho k_n^e)}{Z_{pn}(k_n^e)}\right|^2 + \left(\frac{|d_n|}{\omega\mu_0}\right)^2 \chi_n^{e4}\left|\frac{Z_{pn}(\rho k_n^e)}{Z_{pn}(k_n^e)}\right|^2\right\}.$$

We find for TE_{0m} modes using a similar argument that

$$\alpha_{om_{\text{copper}}} = \frac{\Pi h_m}{\omega\epsilon_0} R_s |N_m|^2\left(\frac{k_m}{k_m^e}\right)^4 J_0^2(k_m) b\left(\frac{|d_m|}{\omega\mu_0}\right)^2 \chi_m^{e4}\left|\frac{Z_{0m}(\rho k)_m^e}{Z_{0m}(k)_m^e}\right|^2$$

and for TM_{0n}

$$\alpha_{on_{\text{copper}}} = \frac{\Pi h_n R_s}{\omega\epsilon_0}|N_n|^2\left(\frac{k_n}{k_n^e}\right)^4 J_0^2(k_n) b\left(\frac{\omega\epsilon_r\epsilon_0}{h_n}\right)^2\left|\chi_n^e\frac{Z'_{pn}(\rho k_n^e)}{Z_{pn}(k_n^e)}\right|^2.$$

The dielectric heat loss may be found in a similar manner as we now have

$$P_L = \frac{1}{2}\int ii^*\rho dV = \frac{1}{2}\int \frac{\sigma E\cdot\sigma E^*}{\sigma}\,dV = \frac{1}{2}\int_0^1\int_0^{2\Pi}\int_a^b \sigma E\cdot E^* r dr d\phi dz$$

where σ is the conductivity of the dielectric. Using field approximations in the lining as given in Unger we have

$$E_r = -V_n A\left[(\chi_n^e S) + \left(\frac{d_n pC}{r}\right)\right]\cos\left[\left(\rho - \frac{r}{a}\right)k_n^e\right]\sin p\phi$$

$$E_\phi = V_n A\left[\left(\frac{pS}{r}\right) - (d_n\chi_n^e C)\right]\sin\left[\left(\rho - \frac{r}{a}\right)k_n^e\right]\cos p\phi$$

$$E_z = jI_n AS\frac{\chi_n^{e2}}{\omega\epsilon_0}\sin\left[\left(\rho - \frac{r}{a}\right)k_n^e\right]\sin p\phi$$

where

$$A \equiv N_n\left(\frac{k_n}{k_n^e}\right)^2 J_p(k_n)$$

$$S \equiv \frac{1}{\sin\delta k_n^e}; \qquad C \equiv \frac{1}{\cos\delta k_n^e}.$$

By substituting for the fields and performing the integration the power loss is obtained. Note that $\sigma = \omega\epsilon_r\epsilon_0 \times$ [lining loss tangent] where ϵ_r is the relative dielectric constant of the lining.

For the TE_{pn} or TM_{pn} modes

$$\alpha_{pn_{\text{dielectric}}} = \frac{\Pi h_n}{2}[\epsilon_r(\text{loss tangent})]|N_n|^2\left(\frac{k_n}{k_n^e}\right)^4 J_p^2(k_n)$$
$$\times\left\{\frac{(\delta+2)\delta k_n^{e2}}{4}\left[S^2\left(1+\frac{\chi_n^{e2}}{h_n^2}\right)+C^2|d_n|^2\right]\right.$$
$$+\tfrac{1}{4}[k_n^e\sin 2\delta k_n^e + \tfrac{1}{2}(1-\cos 2\delta k_n^e)]$$
$$\times\left[S^2\left(1-\frac{\chi_n^{e2}}{h_n^2}\right)-C^2|d_n|^2\right]+SC[\text{Re}\,(d_n)]p\sin 2\delta k_n^e$$
$$\left.+\frac{p^2}{2k_n^e}[\delta k_n^e(S^2+C^2|d_n|^2)+\tfrac{1}{2}\sin 2\delta k_n^e(-S^2+C^2|d_n|^2)]\right\}.$$

We find for TE_{om} modes that

$$\alpha_{om_{\text{dielectric}}} = \Pi h_m[\epsilon_r(\text{loss tangent})]|N_m|^2\left(\frac{k_m}{k_m^e}\right)^4 J_0^2(k_m)\frac{C^2|d_m|^2}{4}$$
$$\times[(\delta+2)\delta k_m^{e2} - k_m^e\sin 2\delta k_m^e - \tfrac{1}{2}(1-\cos 2\delta k_m^e)]$$

and for TM_{0n} modes

$$\alpha_{0n_{\text{dielectric}}} = \frac{\Pi h_n}{4}\left[\epsilon_r(\text{loss tangent})\right]|N_n|^2\left(\frac{k_n}{k_n^e}\right)^4 J_0^2(k_n)$$
$$\times S^2\left\{(\delta+2)\delta k_n^e\left(1+\frac{\chi_n^{e2}}{h_n^2}\right)+\left[k_n^e\sin 2\delta k_n^e\right.\right.$$
$$\left.\left.+\tfrac{1}{2}(1-\cos 2\delta k_n^e)\right]\left(1-\frac{\chi_n^{e2}}{h_n^2}\right)\right\}.$$

APPENDIX B

Wall Impedance Formulation

The determination of the wall impedance (Z_z and Z_ϕ) are discussed in Section III of the text. Here, we will outline the derivation of the eigenvalue equation and the subsequent determination of the propagation and attenuation constants. The boundary conditions at $r = a$ are

$$\begin{aligned} Z_\phi &= E_\phi/H_z|_{r=a} \\ Z_z &= -E_z/H_\phi|_{r=a}. \end{aligned} \tag{30}$$

As before, we can express the fields in the simplified wall impedance structure of Fig. 2 as a superposition of two scalar functions.

$$\begin{aligned} T_n &= N_n J_p(\chi_n r)\sin p\phi \\ T_n' &= N_n J_p(\chi_n r)\cos p\phi. \end{aligned} \tag{31}$$

Here p is an integer, and we must solve a suitable eigenvalue equation to determine χ_n, as before

$$\chi_n a = k_n \tag{32}$$

and γ_n the longitudinal propagation constant is given by

$$\chi_n^2 = k^2 - \gamma_n^2. \tag{33}$$

The tangential fields at the wall ($r = a$) are given by

$$\begin{aligned} E_\phi &= V_n\left[\frac{\partial T_n}{r\partial\phi} - d_n\frac{\partial T_n'}{\partial r}\right]\Bigg|_{r=a} e^{-jh_n z} \\ E_z &= j\omega u_0 I_n\frac{\chi_n^2}{k^2}T_n\Bigg|_{r=a} e^{-jh_n z} \\ H_\phi &= I_n\left[\frac{\partial T_n}{\partial r} + d_n\frac{h_n^2}{k^2}\frac{\partial T_n'}{r\partial\phi}\right]\Bigg|_{r=a} e^{-jh_n z} \\ H_z &= j\omega\epsilon_0 V_n d_n\frac{\chi_n^2}{k^2}T_n'\Bigg|_{r=a} e^{-jh_n z}. \end{aligned} \tag{34}$$

On applying the boundary conditions (30) we obtain the desired eigenvalue equation

$$j\omega\epsilon_0 aZ_z - \frac{k_n J_p(k_n)\left[J'_p(k_n) + j\omega\epsilon_0 Z_\phi \frac{\chi_n}{k^2} J_p(k_n)\right]}{-\frac{p}{k_n^2}\frac{h_n^2}{k^2} J_p^2(k_n) + J'_p(k_n)\left[J'_p(k_n) + j\omega\epsilon_0 Z_\phi \frac{\chi_n}{k^2} J_p(k_n)\right]} = 0$$

where $J'_p(k_n)$ is defined

$$J'_p(k_n) = \frac{d}{dx} J_p(x)\Big|_{x=k_n} . \tag{35}$$

The solutions (k_n) of this equation were determined numerically on a digital computer using a Newton-Raphson iterative scheme. The wall impedances Z_z and Z_ϕ are complex for the most general type of wall impedance waveguide as is the eigenvalue k_n. On determination of k_n, we obtain the complex propagation constant γ_n from (33). The attenuation constant α_n (propagation constant h_n) is then simply the imaginary (real) part of γ_n.

REFERENCES

1. Bucholz, H., "Der Hohlleiter von Kreisformischem Overschnitt mit Geschichtetem Dielektrischen Einsatz," Ann. Phys., *43*, 1943, pp. 313–368.
2. Wachowski, H. M., and Beam, R. E., "Shielded Dielectric Rod Waveguides, Final Report on Investigation of Multi-Mode Propagation in Waveguides and Microwave Optics," Microwave Laboratory, Northwestern University, Ill., 1950.
3. Unger, H. G., "Circular Electric Wave Transmission in a Dielectric Coated Waveguide," B.S.T.J., *36*, No. 5 (September 1957), p. 1253.
4. Unger, H. G., "Lined Waveguide," B.S.T.J., *41*, No. 2 (March 1962), p. 745.
5. Carlin, J. W., and D'Agostino, P., "Low-Loss Modes in Dielectric Lined Waveguide," B.S.T.J., *50*, No. 5 (May-June 1971), p. 1631.
6. Carlin, J. W., and Maione, A., "Experimental Verification of Low-Loss TM Modes in Dielectric-Lined Waveguide," B.S.T.J., this issue, pp. 487–496.